Ion Conduction Mechanism as a Fingerprint of Potassium Channels

Ion conduction mechanism is a fingerprint of potassium channels

Carmen Domene[1,2], Riccardo Ocello[3], Matteo Masetti[3], Simone Furini[4*]*

[1]Department of Chemistry, University of Bath, Claverton Down, Bath, BA2 7AY, UK

[2]Department of Chemistry, University of Oxford, Mansfield Road, Oxford, OX1 3TA, UK

[3]Department of Pharmacy and Biotechnology, Alma Mater Studiorum – Università di Bologna, via Belmeloro 6, 40126 Bologna, Italy

[4]Department of Medical Biotechnologies, University of Siena, Siena, Italy

Running title: Conduction in K^+-channels

Keywords: conduction mechanisms; ion permeation; molecular dynamics simulations; ion channels; inactivation; KcsA; TRAAK

* Corresponding authors

Simone Furini - simone.furini@unisi.it

Carmen Domene - c.domene@bath.ac.uk

Abstract

K+-channels are membrane proteins that regulate the selective conduction of potassium ions across cell membranes. Although the atomic mechanisms of K+ permeation have been extensively investigated, previous work focused on characterizing the selectivity and occupancy of the binding sites, the role of water molecules in the conduction process, or the identification of the minimum energy pathways enabling permeation. Here, we exploit molecular dynamics simulations and the analytical power of Markov state models to perform a comparative study of ion conduction in three distinct channel models. Significant differences emerged in terms of permeation mechanisms and binding site occupancy by potassium ions and/or water molecules from 100 μs cumulative trajectories. We found that, at odds with the current paradigm, each system displays a characteristic permeation mechanism, and thus, there is not a unique way by which potassium ions move through K+-channels. The high functional diversity of K+-channels can be attributed in part to the differences in conduction features that have emerged from this work. This study provides crucial information and further inspiration for wet-lab chemists designing new synthetic strategies to produce versatile artificial ion channels that emulate membrane transport for their applications in diagnosis, sensors, the next generation of water treatment technologies, etc., as the ability of synthetic channels to transport molecular ions across a bilayer in a controlled way is usually governed through the choice of metal ions, their oxidation states, or their coordination geometries.

Introduction

K+-channels are a vast and heterogeneous family of membrane proteins. They control the passage of ions across cell membranes, and by doing so, they contribute to numerous biological functions, as diverse as cellular homeostasis, the transmission of nerve impulses, or the regulation of cardiac activity. Inspired by the structures, properties, and functions of cellular ion channels, chemists have been making synthetic mimetics to facilitate the understanding of nature's principles or to exploit nature's designs characterized by high selectivity and permeability.1–5 It is not surprising that the functional features of K+-channels are highly heterogeneous considering the diversity of their biological roles. K+-channels differ from each other by the stimuli that control the opening and closing of the pore, which is sometimes used to classify them in mechanosensitive, ligand-gated, and voltage-gated ion channels.

Another feature that defines K+-channels is their ability to inactivate or not, and the time constant that characterizes this process, which expands from a few microseconds to seconds. Conductance also expands over a wide range of values, from a few to hundreds of picosiemens. Over the last 20 years, the atomic structures of numerous K+-channels have been experimentally resolved by X-ray crystallography and, more recently, by cryo-electron microscopy. These models allow research that contributes to knowledge about the mechanisms underlying how K+-channels work, from which we can deduce the possible determinants of their functional diversity. However, in contrast to the static information contributed by structural work, gating, inactivation, and conduction are intrinsically dynamical processes, and, thus, these regulatory mechanisms cannot be solely addressed by structural approaches. Computational methods, in particular molecular dynamics (MD) simulations, have proven to be a valuable tool to explore the properties of ion channels at the atomic scale, complementing structural and physiological studies.6–11 MD simulations have been steadily revealing atomic details of conduction and selectivity in K+-channels.12–15 However, the degree of similarity in permeation strategies between members of the K+-channel family remains to be established. In this study, MD simulations were used to compare and contrast the mechanisms characterizing conduction in three prototypical K+-channels.

The selective conduction of ions across K+-channels is controlled by the selectivity filter (SF), which is a 10–12 Å long narrow pore at the extracellular side of the protein (Figure1). The SF is

composed of four consecutive potassium binding sites, which are known as S1, S2, S3, and S4, starting from the extracellular side. At each of these binding sites, a potassium ion is sandwiched between two layers of four oxygen atoms contributed by the backbone of the SF residues, with the exception of S4, where one of these layers is contributed by the side chain of the corresponding residues at the N-terminal of the SF sequence. At the extracellular side, an external site, S0, has also been identified, and the ion at this site is also coordinated by oxygen atoms, which are in part contributed by water molecules. At the intracellular side, the pore opens into a water-filled cavity. In the open conformation of the channel, the water-filled cavity extends to the intracellular media. In contrast, in the closed conformation, the helix-bundle crossing gate formed by the cytoplasmic side of the TM2 or TM6 helices of the pore-domain seals the connection of the cavity with the intracellular media.

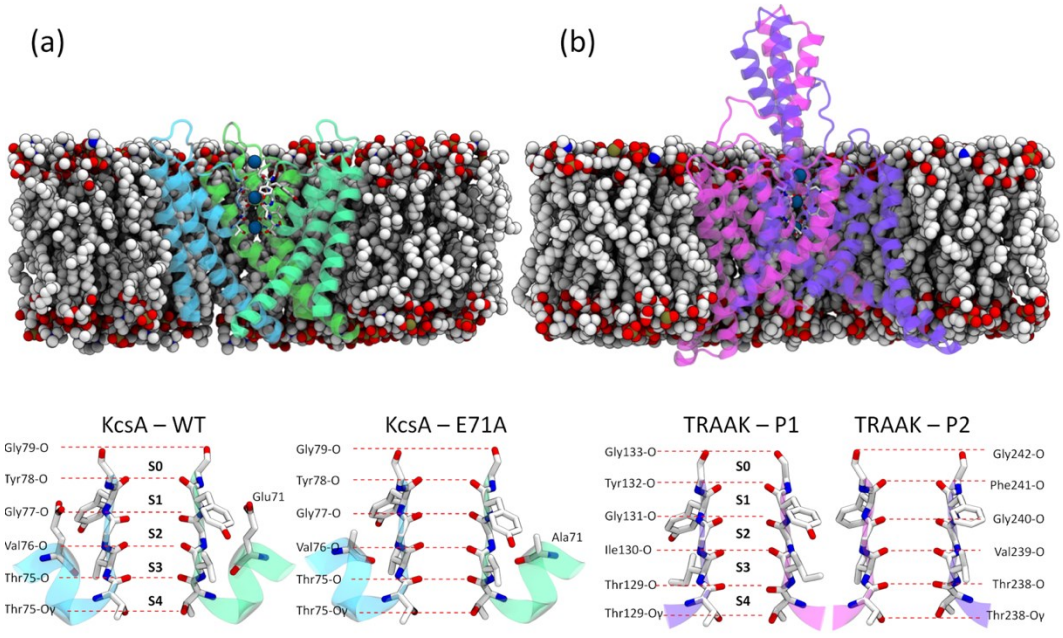

Figure 1. Illustration of the (a) KcsA and (b) TRAAK channels. Top panels: Simulation systems with the proteins shown in cartoon representations and the lipids and K+ as VDW spheres. Bottom panels: Two opposing subunits of the selectivity filter of KcsA-WT, KcsA-E71A, and TRAAK are shown in licorice representations with labels indicating binding sites S0–S4. In KcsA-WT and KcsA-E71A, residue 71 is also shown in licorice representation. Two orthogonal views of the SF are shown for the TRAAK channel, as TRAAK is a dimer-of-dimers with two pairs of identical monomers in pink and purple, each contributing to the selectivity filter with two different sequences, TIGYG and TVGFG.

At physiological conditions, the electrochemical gradient drives K+ from the intracellular to the extracellular side. Originally, conduction of K+ was described as the concerted movement of a single file of ions and water molecules across the SF, where two ions were separated by an intervening water molecule.6,7,16,17 According to this conduction mechanism, the SF mainly exists in two states, with ions respectively in S2 and S4 and water molecules in S1 and S3, or ions in S1 and S3 and water molecules in S2 and S4. A conduction event in the outward direction is initiated by an ion moving from the intracellular cavity into S4, prompting the concerted displacement of ions (and water) already inside the SF from S3−S1 to S2−S0. The displacement of the outermost ion from S0 to the extracellular solution concludes the conduction event. Subsequently, the viability of an alternative conduction strategy to the classical "knock-on" mechanism with ions separated by water molecules was presented and justified by energetic calculations.10 In this alternative strategy, ions can travel through the SF without intervening water molecules, with the implication that empty binding sites emerge. MD simulations that mimicked electrophysiological experiments by imposing a drifting force between the intracellular and the extracellular side of the channel also reported conduction events in the absence of water molecules, with the caveat that this mechanism was presented as an exclusive rather than an alternative one to the "knock-on" mechanism.11 The water-free conduction mechanism is in agreement with solid state NMR experiments,18 while it is at odds with experimental streaming potential measurements, which support instead the cotransport of water molecules and ions.19 The absence of water molecules from conduction events was also associated20 with the selectivity of K+ over Na+. If selectivity requires water-free conduction, the absence of water molecules from the core of the SF is expected to be a common feature shared by the entire channel family. In this context, while certain characteristics of conduction are likely to be conserved across K+-channels, such as the number and the structural characteristics of the ion binding sites, or the involvement or not of water molecules in permeation events, other features, such as the percentage occupancy of the SF, might be different among different channels, in particular, if proteins with different SF sequences are compared. The presence of alternative conduction strategies in K+-channels is an intriguing biophysical question, with important implications for our understanding of the functioning of ion channels and the factors responsible for their functional diversity. For instance, experimental data have shown that ion binding at the SF impacts C-type inactivation.21,22 Therefore, because alternative conduction strategies are likely to be

characterized by different degrees of occupancy of binding sites S0–S4 either by ions and/or water molecules, differences in conduction could be responsible for the heterogeneous characteristics of C-type inactivation among K+-channels. More generally, as the loading state of the SF is likely to alter the dynamical properties of the protein, the particular conduction strategy adopted by a particular K+- channel might help explain its peculiar functional characteristics, not only in terms of conductivity but also with respect to gating, inactivation, and drug modulation.

In the present study, MD simulations were performed for three distinct channel models, corresponding to the wild-type bacterial KcsA channel (KcsA-WT), the Glu71Ala KcsA mutant (KcsA-E71A), and the eukaryotic two-pore domain Twik-related arachidonic acid K+-channel (TRAAK). KcsA has been used as a prototype in a large number of computational studies of K+-channels since the availability of its experimental structure back in 1998.23 KcsA is gated by pH, and upon a sustained pH stimulus, it inactivates via a process that resembles C-type inactivation of eukaryotic K+-channels.24 The glutamate 71 to alanine mutation abolishes inactivation in KcsA.25 Therefore, by comparing KcsA-WT and KcsA-E71A, it will be possible to reveal differences in the conduction strategy between a channel that undergoes inactivation (wild-type KcsA) and one that cannot inactivate (mutant) with otherwise minimal structural variations. In contrast, the TRAAK channel was included in the study as an outlier compared to KcsA-WT and KcsA-E71A. Conversely to other K+-channels, two-pore domain K+-channels are constituted by two, rather than four, protein chains, each of them contributing with two subunits to the central pore.26 In TRAAK, the sequence of the SF is different between the two adjacent subunits, and both diverge from the canonical TVGYG signature sequence common to most K+-channels, being TIGYG and TVGFG respectively (Figure 1).

The hypothesis that we wanted to test in this study was if different K+-channels adopt different conduction strategies or not. In order to assess this hypothesis, extensive MD simulations were executed to estimate Markov state models (MSMs) for conduction events. Comparison of the MSMs rendered for KcsA-WT, KcsA-E71A, and TRAAK demonstrates that the preferential conduction mechanism in potassium channels is indeed channel specific.

Materials and Methods

Atomic model

The KcsA atomic models were based on the experimental structure of the channel in the open/conductive state, Protein Data Bank entry 5VK6.27 The model of the TRAAK channel was based on the Protein Data Bank entry 4WFE.28 In both cases, KcsA and TRAAK, the entire transmembrane domain of the channel was considered in the models, from residue Trp26 to residue Gln121 in the case of KcsA and from residue Arg2 to residue Arg284 in the case of TRAAK. The initial atomic coordinates of the simulated systems were defined using CHARMM-GUI.29 The channel was inserted in the lipid membrane as defined in the Orientations of Proteins in Membranes (OPM) database.30 In KcsA-WT and KcsAE71A, the lipid membrane was a mixture of 1-palmitoyl-2-oleoylglycero-3-phosphocholine (POPC) and 1-palmitoyl-2-oleoyl-sn-glycero-3-phosphate (POPA) in a 3 POPC:1 POPA ratio. In TRAAK, the lipid membrane was modeled as pure POPC, as commonly adopted in other MD simulations of mechanosensitive channels.31,32 The difference in lipid composition between the KcsA and TRAAK models is not expected to significantly affect the conduction properties in the simulated time scales.33 The systems were solvated using TIP3P water molecules34 amounting to ∼15 000 and ∼28 000 molecules for KcsA and TRAAK, respectively. Ions were added to achieve a concentration of 200 mM of KCl. Potassium ions were manually placed at binding sites S4, S2, and S0. The ff14sb version of the AMBER force field was used35 in combination with ion parameters for the TIP3P water model by Joung and Cheatham.36 van der Waals interactions were truncated at 9 Å. Standard AMBER scaling of 1−4 interactions was applied. The atomic systems were equilibrated in consecutive steps of 5, 5, 5, 40, 10, 10, and 10 ns with harmonic restraints applied on the distance along the z-axis (channel axis) of the center of mass of the lipid headgroups and on the root mean square deviation of the protein backbone and side chain heavy atoms from their initial configuration, with force constants of 5 kcal·mol−1·Å−2 for lipid headgroups, 10 kcal·mol−1·Å−2 for backbone atoms, 5 kcal·mol−1·Å−2 for protein side chain atoms; then decreased to 5, 5, 2.5 kcal·mol−1·Å−2; 2, 2.5, 1 kcal·mol−1·Å−2; 1, 1, 0.5 kcal·mol−1·Å−2; 0.2, 0.5, 0.1 kcal·mol−1·Å−2; 0, 0.1, 0 kcal·mol−1·Å−2; and 0, 0, 0 kcal·mol−1·Å−2. A time step of 1 fs was used for the first three equilibration trajectories and of 2 fs for the remaining ones. Long-range electrostatic interactions were calculated with the particle mesh Ewald method using a grid spacing of 1.0 Å.37 The SETTLE algorithm was used to restrain bonds with the

hydrogen atom.38 The temperature was maintained at 310 K by coupling the system to a Langevin thermostat with a damping coefficient of 1 ps−1. A pressure of 1 atm was kept during the simulation by coupling the system to a Nosé−Hoover Langevin piston with a damping constant of 25 ps and a period of 50 ps.39 The presence of membrane potentials was mimicked by applying a constant electric field acting along the axis of the simulation box perpendicular to the lipid membrane. The simulations with externally applied electric fields were performed in the NVT ensemble as previously described.40,41 NAMD2.12 was used for all the simulations.42 The total simulation time was over 100 μs.

Analysis

Trajectories were analyzed using the python library MDanalysis43 and the SciPy ecosystem.44 Visual Molecular Dynamics (VMD) was used to inspect trajectories and to generate images of the systems.45 In the simulations of KcsA-WT and KcsA-E71A, the centers of mass of the following set of atoms were considered as boundaries for the different channel regions: residues Ala107 (SClow), the hydroxyl oxygen atom of residues Thr75 (S4low), the backbone oxygen atom of residues Thr75 (S3low), backbone oxygen atom of residues Val76 (S2low), the backbone oxygen atom of residues Gly77 (S1low), the backbone oxygen atom of residues Tyr78 (S0low), and the backbone oxygen atom of residues Gly79 (S0high). Analogous sets of atoms were used as boundaries for the TRAAK channel: residues Leu161 and Leu276 (SClow), the hydroxyl oxygen atom of residues Thr129 and Thr238 (S4low), the backbone oxygen atom of residues Thr129 and Thr239 (S3low), backbone oxygen atom of residues Ile130 and Val239 (S2low), the backbone oxygen atom of residues Gly131 and Gly240 (S1low), the backbone oxygen atom of residues Tyr132 and Phe241 (S0low), and the backbone oxygen atom of residues Gly133 and Gly242 (S0high). Potassium ions or water molecules were considered inside the cavity when their coordinates along the axis of the channel pore were in between SClow and S4low. The same protocol was applied to identify if an ion or a water molecule occupies binding sites S0−S4. Ions and water molecules were considered in binding sites S0−S4 or in the cavity only when they were within 4 and 8 Å from the channel axis, respectively. Using these binding site definitions, each frame of the simulated trajectories was converted into a string describing the occupancy for a posteriori classification.

The occupancy state of the channel in each frame of each trajectory was case coded using the following regular expression: [Kw][Kw−]-[Kw−][Kw−][Kw−][Kw−]. The first character of the

string was K when a potassium ion was inside the cavity (between SClow and S4low) or w otherwise, if the cavity was only filled with water molecules. Similarly, the next character of the string was K if S4 was occupied by an ion, w if it was occupied by a water molecule, and – if S4 was vacant. To define the characters describing binding sites S3 to S0, the same criteria were imposed. At times, due to the intrinsic structural nature of S0, an ion and a water molecule can coexist at S0, and thus, in this particular case, the character K was selected. This classification of the occupancy state of the channel was used to convert the simulated trajectories into sequences of discrete states to be used to estimate MSMs representing the transitions between different occupancy states of the SF.

MSMs were computed for KcsA-WT, KcsA-E71A, and TRAAK using data from simulations with a membrane potential equal to +200 mV. The transition matrix among these discrete states of the channel was calculated as

$$T_{ij} = \frac{C_{ij}}{\sum_k C_{ik}} \quad (1),$$

where Tij is the estimated probability of moving from state i to state j during the sampling period, and Cij is the number of transitions observed between the same two discrete states during the whole simulation time. The transition matrix of an MSM has an eigenvalue equal to 1, with the corresponding eigenvector providing the equilibrium probability.46 The other eigenvalues, λi, have a norm lower than 1, and the corresponding eigenvectors describe deviations from this equilibrium probability that decay with a relaxation time ti, defined as

$$t_i = -\frac{\tau}{\ln|\lambda_i|} \quad (2),$$

with τ being the sampling period, sometimes referred to as the lag time of the MSM. Relaxation times were estimated for different sampling periods in order to verify the validity of the Chapman–Kolmogorov equation. Since MSMs were estimated using trajectories in the presence of an external electric field, the transition matrix is not expected to obey detailed

balance, and net fluxes are possible between pairs of connected states. The net flux between any pair of states, fij, was calculated as

$$f_{ij} = T_{ij}p_i - T_{ji}p_j \quad (3),$$

where pi is the estimated probability of state i. In order to estimate the uncertainty affecting the state probabilities and the net fluxes, the MSM of each model system was computed 10 times using different random subsets of the trajectories that included only half of the simulated trajectories (four trajectories for KcsA-WT and KcsA-E71A, six trajectories for TRAAK). State probabilities and net fluxes were well conserved among these different MSMs, confirming that the estimated parameters do not depend on the initial conditions of the simulated trajectories. State probabilities and net fluxes are reported as average and standard deviations computed from estimates based on different subsets of trajectories. The Kruskal–Wallis test in combination with the Dunn posthoc test was used to compare binding site occupancies of the three model systems. Graph images were generated with Gephi.4

Results and Discussion

A water-depleted filter is a requirement to observe ion conduction

MD simulations were performed for the three channel models considered, KcsA-WT, KcsA-E71A, and TRAAK, at membrane potentials equal to +100 and +200 mV and considering two initial states of the SF, with and without water molecules, respectively. At least three independent trajectories were simulated for each combination of (i) channel model, (ii) loading state of the SF, and (iii) membrane potential (Tables S1–S3 in the Supporting Information). The simulations where ions were initially placed in binding sites S0, S2, and S4, and water molecules in S1 and S3, will be described first. In these simulations, the analysis of the water stability inside the SF revealed remarkable differences among the three systems considered. In KcsA-WT, the initial configuration of the SF was stable for most of the simulated trajectories. Water molecules inside the SF remained at their initial positions in each of the four 1 μs trajectories at +100 mV, and, consequently, conduction was not observed. Similarly, at the higher membrane potential of +200 mV, no conduction event was observed in three out of the four trajectories. In the remaining trajectory, an outward movement of ions and water molecules

was observed between 100 and 200 ns. This event caused the exit of water molecules initially in S3 and S1 from the SF, after which no water molecules occupied binding sites S3 and S2. This trajectory was the only one where a few ion conduction events were observed, and so, it seems as if the presence of water molecules in the core of the SF (sites S3 and S2) was preventing conduction. Likewise, water molecules occupying S3 and S1 blocked conduction in KcsA-E71A. However, while in KcsA-WT extrusion of water molecules from the SF was a rare event on the simulated time scale, in KcsA-E71A, water molecules were expelled from the core of the SF in less than 100–300 ns in all trajectories, both at +100 and +200 mV. From this standpoint, no water molecule was observed in binding sites S3 and S2. In terms of water extrusion from the SF, the events recorded for TRAAK were an intermediate situation between those observed in KcsA-WT and KcsA-E71A; water molecules were expelled from the SF only in half of the trajectories, and these events took place on longer time scales compared to the events recorded for KcsAE71A. However, as in KcsA-WT and KcsA-E71A, conduction events were observed only in the absence of any water molecule in the SF core. These data support our previous observations,48,49 and they are in line with recent literature.18 The conduction mechanism and, consequently, the presence or absence of water molecules might depend on the adopted force field. Recently, we showed that in microsecond trajectories with the CHARMM36 force field the SF evolves toward a nonconductive state in hundreds of nanoseconds, both in KcsA (wild type and mutant) and TRAAK.48,49 As a consequence, the AMBER-ffsb14 force field, which instead was shown to preserve the conductive state of the SF as expected in microsecond-long trajectories, was used for all the simulations considered here. In summary, MD simulations initialized from different loading states of the SF in terms of water occupancy support the hypothesis that a water-depleted SF is a common feature of ion conduction among different types of K+-channels (for simplicity, hereafter referred to as water-free conduction).

The loading states of the selectivity filter are channel-specific

Since water-free conduction emerged as the preferred mechanism in the three systems simulated, alternative simulations were considered for TRAAK and KcsAWT, starting from an initial configuration of the SF with ions at S0, S2, and S4 and gaps at S1 and S3 (Tables S1–S3 in the Supporting Information). In the case of KcsA-E71A, water exits fast from the SF, and subsequently, water-free conduction was established in all the trajectories. For this reason, it

was not necessary to perform an independent set of simulations of KcsA-E71A initialized without water molecules inside the SF. The analyses presented next are based on the simulations of TRAAK and KcsA-WT initialized without water molecules inside the SF and the portion of the trajectories of the KcsAE71A system after water molecules had escaped from the SF.

The estimated conductance recorded at +200 mV was similar for the three channel models: 8.0 ± 1.0 pS for KcsAWT, 9.0 ± 1.2 pS for KcsA-E71A, and 4.5 ± 1.6 pS for TRAAK. The uncertainty on the conductance values was calculated as the standard deviation among the estimates obtained from independent trajectories. As previously reported,49,50 the predicted conductance underestimates the experimental data in all the cases by more than 1 order of magnitude. The reasons for this quantitative disagreement between MD simulations and experimental data could be ascribed to the differences between the in-silico models and the experimental setups such as membrane composition and/or protocol used to apply the membrane potential, to possible limitations of the force field employed, or, more likely, to a combination of several of these factors. Overall, MD simulations of KcsA-WT, KcsA-E71A, and TRAAK revealed that, regardless of the channel, sites S2 and S3 are occupied by potassium ions with high probability, and consequently, they are rarely occupied by water molecules. Data extracted from simulations at +200 mV are summarized in Figure 2 and Table 1 and discussed next. Similar distributions were observed in simulations at +100 mV, and they are reported in Figure S1 of the Supporting Information. In KcsA-WT, binding sites S0, S1, and S4 have similar probabilities to be occupied by K+, close to 15−20%, while the probability to be occupied by water molecules is close to 40% for S4 and approximately 70−80% for S0 and S1. Thus, the SF of KcsA-WT is characterized by a central core, sites S3 and S2, which favors ions, and at either side of this central core, sites occupied by water molecules with high probability. In addition, the intracellular cavity of KcsAWT hosts an ion with a probability close to 60%, and for most of the simulated time, this ion stays close to the lower boundary of S4.

The occupancy of binding sites by ions and water molecules is similar in KcsA-WT and KcsA-E71A, with a few remarkable differences. The probability that S0 is occupied by an ion is significantly higher in KcsA-E71A (∼60%) than in KcsA-WT (<20%). The higher degree of ion occupancy of S0 in KcsAE71A compared to KcsA-WT could be explained by the fact that the Glu71Ala mutation abolishes any possible interaction between residues at position Glu/Ala71

and Tyr78 (Figure 1). In KcsA-WT, the side chain carboxyl oxygen atoms of Glu71 interact electrostatically with the backbone amide group of residues Tyr78 (Figure S2), while in KcsA-E71A, Tyr78 is not restrained by interactions with Ala71, which results in a slight modification of the G77 and Y78 backbone angles (Figure S3). Moreover, the mutation Glu71Ala modifies the position along the channel axis of the side chain oxygen atoms of residues Asp80 (Figure S4), which might impact on the electrostatic properties of binding sites S1 and S0. Other differences between KcsA-WT and Kcsa-E71A can be correlated to the distinct behavior of S0. For example, the probability of finding an ion in S1 is lower for KcsA-E71A (<5%) than for KcsA-WT (∼15%). In addition, the absence of an ion at S1 further stabilizes ions at S3 and S2. Indeed, while in KcsA-WT ion movements between S3 and S4 are frequently observed, in KcsA-E71A the ion at S3 is stable, and the probability of observing an ion at S4 is consequently lower, being around 15% in KcsA-WT and <5% in KcsA-E71A. These differences in ion occupancy also have an effect on the binding of water molecules in the SF. The probability of recording water molecules is lower in KcsA-E71A compared to KcsA-WT (Table 1).

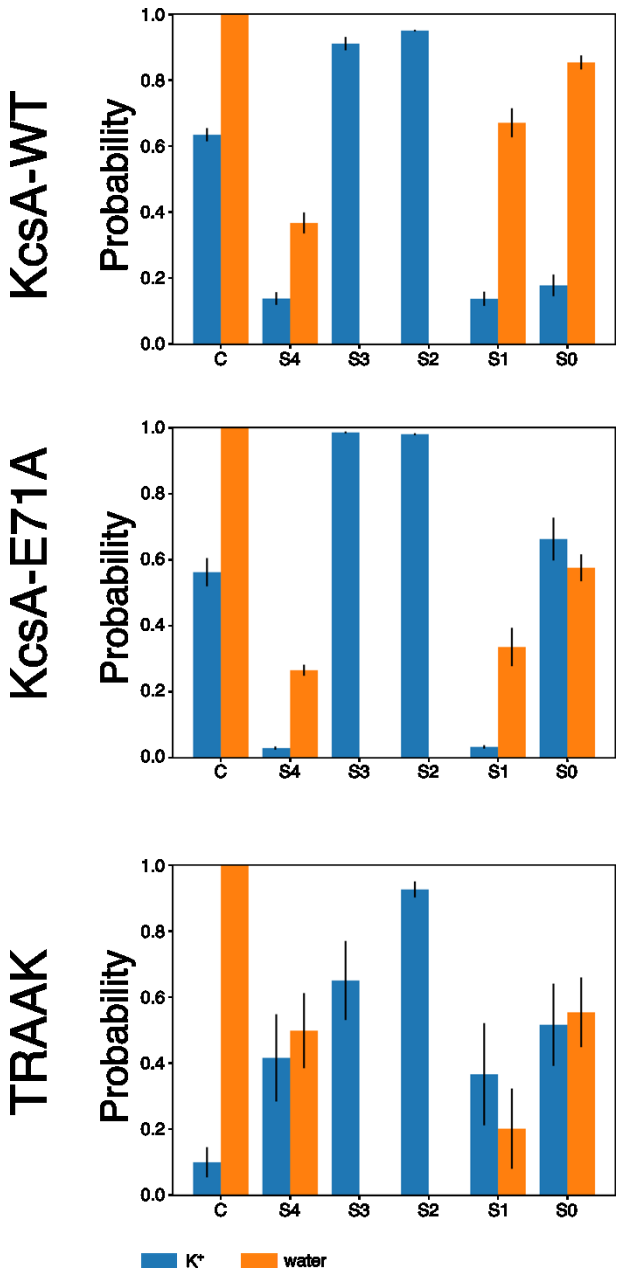

Figure 2. Potassium ions and water molecules inside the selectivity filter. Ions and water molecules were considered in a binding site when they occupy the space in-between the two layers of oxygen atoms delimiting the corresponding binding site. Binding sites S3 and S2 are vacant if they are not occupied by K+; regardless of the channel model and membrane potential, water never occupied S2 or S3. The intracellular cavity, C, is always filled with several water molecules, and consequently the water probability is identical to 1. The cavity and S0 are wide enough to accommodate both water molecules and ions. Data from simulations with membrane potentials equal to +200 mV and initialized without water molecules inside the SF (TRAAK and KcsA-WT) or after the exit of water molecules from the SF (KcsA-E71A) were used to calculate ion/water occupancy probabilities. Average values (bars) and standard deviations (vertical lines) were computed using data from independent trajectories.

Table 1. Average Occupancy of the Selectivity Filter Binding Sites (S0–S4) and of the Intracellular Cavity by K+ and Water (C)a

		Kcsa-WT	KcsA-WT vs KcsA-E71A	KcsA-WT vs TRAAK	KcsA-E71A	KcsA-E71A vs TRAAK	TRAAK
K^+	S0	0.18±0.03	p < 0.01	p < 0.01	0.66±0.07	-	0.53±0.12
	S1	0.14±0.03	-	-	0.03±0.01	p < 0.01	0.35±0.15
	S2	0.94±0.03	p < 0.01	-	0.98±0.01	p < 0.01	0.93±0.02
	S3	0.91±0.03	-	p < 0.01	0.99±0.01	p < 0.01	0.66±0.12
	S4	0.14±0.02	-	p < 0.01	0.03±0.01	p < 0.01	0.40±0.13
	C	0.63±0.01	-	p < 0.01	0.56±0.04	p < 0.01	0.10±0.05
water	S0	0.85±0.02	p < 0.01	p < 0.01	0.58±0.04	-	0.54+0.10
	S1	0.67±0.04	-	p < 0.01	0.34±0.06	-	0.21+0.12
	S2	0	-	-	0	-	0
	S3	0	-	-	0	-	0
	S4	0.37±0.03	-	-	0.26+0.02	p < 0.01	0.52+0.12

a Values from different replicas were used to compute averages and standard deviations and to estimate the statistical significance for the various comparisons. The Kruskal−Wallis statistical test in combination with the Dunn post-hoc test were used. Significant differences with a p-value lower than 0.01 are reported in columns KcsA-WT vs KcsA-E71A, Kcsa-WT vs TRAAK, and KcsA-E71A vs TRAAK, respectively.

Considering the significant differences in terms of ion and water occupancy induced in KcsA by a single amino acid mutation at the back of the SF, it is not surprising that even more significant differences are observed between KcsA and TRAAK. The only common characteristic between TRAAK and KcsA trajectories is the absence of water molecules at binding sites S2 and S3. However, while in KcsA-WT and in KcsA-E71A the ion occupancy is similar at these binding sites, in TRAAK, the ion occupancy is lower at S3 (∼70%) compared to S2 (∼90%). The lower probability of ion binding at S3 in TRAAK compared to both KcsA-WT and KcsA-E71A is correlated with a higher probability of finding an ion at S4 and, consequently, to a lower probability of finding an ion in the cavity. Notably, these occupancies are in good agreement

with those previously reported for the same channel, which were found to be 46%, 65%, 97%, and 58% for the S4, S3, S2, and S1 binding sites, respectively.51 At the extracellular entrance of the channel, binding sites S0 and S1 in TRAAK present the highest cumulative ion occupancy among the three simulated systems and, consequently, the lowest probability to observe water molecules.

In summary, the binding of ions and water molecules is channel specific, and this is reflected in the different average number of ions and water molecules inside the SF, being respectively 2.87 and 1.25 in TRAAK, 2.69 and 1.18 in KcsAE71A, and 2.32 and 1.89 in KcsA-WT.

Characterization of the dominant mechanisms of conduction

The different loading states of the SF suggest the adoption of different conduction strategies by different channels, and, indeed, the possibility of alternative strategies is clearly confirmed by the time series of ion conduction events. Representative examples of conduction events for the three models considered are reported in Figure 3. While these plots can be highly informative to grasp the overall dynamics of the ions in the SF and to find out differences at a qualitative level, they cannot provide a detailed mechanistic description of ion conduction. Therefore, to go beyond a purely anecdotal description of events, Markov state models were built to describe conduction events for each channel model. For the definition of these MSMs, the simulated trajectories were converted into sequences of discrete states. These discrete states were defined considering the loading states of the central cavity and binding sites S4–S0. For instance, all the time points when (i) the cavity, S3, and S2 were occupied by an ion, (ii) S4 and S0 were occupied by water, and (iii) S1 was empty had a unique identifier assigned to them, and similarly for all the possible loading states sampled in the trajectories. Subsequently, the discretized trajectories were used to estimate the transition matrix for each of the MSMs associated with the three model systems.

To correctly describe the process under investigation by an MSM, it is necessary that transitions among discrete states are memoryless. The standard method described in the literature to check this feature is a comparison of the relaxation times estimated from MSMs obtained at different sampling periods. Based on the Chapmann–Kolmogorv equation, these relaxation times should be independent of the sampling period. For the discretization procedure described above, this condition is satisfied in the three models when the sampling times are over 4 ns (Figures S5); this sampling period was consequently used to estimate the

MSMs for conduction events. The advantage of a piece of analysis based on MSMs is that trajectories from different replicas can easily be combined to estimate a consensus description of conduction events, which can then be compared in quantitative terms.

The complete networks of SF states obtained from the transition matrix of the MSMs are illustrated in Figures S6–S11. For the sake of clarity, a simplified schematic representation is also provided in Figure 4 and Tables S4 and S5. The simplified network shown in Figure 4 was obtained by merging nodes with the same configuration of ions, regardless of the presence or absence of water molecules. The same conduction events illustrated in Figure 4 can be retrieved from the complete networks included in the Supporting Information. In the jargon of network analysis, the occupancy states of the channel correspond to the nodes of a graph, and the net fluxes correspond to the edges of the graph. The graphs illustrated in Figure 4, which provide a schematic and simplified representation for the transition matrices of the MSMs, show that conduction can be accomplished in several different ways. In particular, since ion conduction is a cyclic process, every closed path between the nodes of the directed networks entails a distinct mechanism characterized by (i) an ordered sequence of detectable configurations of the SF, (ii) an associated probability to visit these states, and (iii) a net flux quantifying the relative probability to reach the next state starting from the current one. It is important to note that such a mechanistic description of ion conduction is subjected to the temporal resolution limit imposed by the sampling period used to build the MSMs (4 ns in our case). Overall, this analysis demonstrates that, in each of the channels considered in this study, ion conduction takes place competitively via several mechanisms. The MSMs allow quantitatively characterization of the most probable path (highest net flux) connecting the most populated states, leading to the identification of a prevailing strategy of ion conduction for every channel (hereafter referred to as the "dominant" mechanism). Crucially, the dominant mechanism turns out to be significantly different in KcsA-WT, KcsA-E71A, and TRAAK.

In KcsA-WT, the state with the highest probability (52 ± 1%) is characterized by the presence of ions in the cavity, S3, and S2. From that point, conduction is initiated when the ion in the cavity approaches the SF, pushing other ions toward the extracellular side. In Figure 4a, this is represented by the following edges in the graph: (i) [C, S3, S2] → [S3, S2, S0]; (ii) [C, S3, S2] → [S4, S2, S1] → [S3, S2, S0]; and (iii) [C, S3, S2] → [S4, S3, S1] → [S3, S2, S0], where C indicates the presence of an ion in the cavity. These alternative routes are characterized by different net

fluxes, which are reported along the corresponding edges as values normalized to the maximum net flux in the entire network (average and standard deviation computed using MSMs estimated from different sets of simulations). Switching between [C, S3, S2] and [S3, S2, S0] configurations was observed, but obviously, it cannot occur directly and without intermediate steps. This feature is accredited to the temporal resolution of the MSM, which does not allow the detection of transitions that are faster than the sampling period. Even if the fine grained details of the transition between [C, S3, S2] and [S3, S2, S0] are somehow hidden by the sampling period, the magnitude of the net flux along this route is quantified and can be compared with the other two models. Concerning the stepwise transitions, [C, S3, S2] → [S4, S2, S1] → [S3, S2, S0] is characterized by higher net fluxes than [C, S3, S2] → [S4, S3, S1] → [S3, S2, S0]. Once the [S3, S2, S0] configuration is reached, ion conduction proceeds either by first emptying S0 and then accommodating an ion in the cavity or, conversely, by accommodating an ion in the cavity and then vacating S0. These two competing routes are characterized by intermediate states with similar probabilities: [S3, S2], 14 ± 1%, and [C, S3, S2, S0] 10 ± 1%, respectively. The net fluxes along these two routes are also similar. These facts suggest that the transitions are almost equally likely to occur in KcsA-WT.

The same sequence of states described for KcsA-WT is observed for KcsA-E71A. However, the probabilities of these states are broadly different between KcsA-WT and KcsA-E71A, resulting in diverging conduction events, as it is also evidenced from inspection of the representative trajectories illustrated in Figure 3. Notably, in KcsA-E71A, states [C, S3, S2], [S3, S2, S0], and [C, S3, S2, S0], with individual probabilities of 25 ± 2%, 34 ± 1%, and 32 ± 1%, respectively, account for more than 90% of the total probability (Figure 4b and Table S4). This discrepancy is also reflected in changes in the magnitude of net fluxes of the main states. In particular, the transition [S3, S2, S0] → [S3, S2] is significantly reduced in KcsA-E71A compared to KcsA-WT (Table S5), in accordance with the reduced stability of binding site S0 by the E71A mutation. Comparison of the dominant conduction mechanisms in KcsAWT and KcsA-E71A clearly reveals that the system with the mutation cycles between three main states with similar probabilities, while the wild-type channel is overall stable in a single state (panel a versus panel b in Figure 4, or Figures S6 and S7 versus S8 and S9 in the Supporting Information). Consequently, KcsA-E71A adopts a state with at least one ion at S1 or S0 more often than KcsA-WT. The presence of ions in these binding sites prevents water molecules from entering the SF from the

extracellular side, and consequently, the average number of water molecules inside the SF is lower in KcsAE71A compared to KcsA-WT. Moreover, ion conduction in KcsA-WT is characterized by a greater number of competing cycles that are mostly associated with lower fluxes compared to the dominant mechanism. Conversely, in KcsA-E71A, the dominant mechanism captures most of the net fluxes in the network.

The probability of having at least one ion in S1 or S0 is maximum in TRAAK, and in accordance, the TRAAK channel is the one with the lowest number of water molecules at the extracellular binding sites of the SF among the three simulated systems (Figure 2). In striking contrast to the other investigated channels, configuration [C, S3, S2] is observed with 3.7 ± 0.7% probability in TRAAK compared to 52% and 25% in KcsA-WT and KcsA-E71A, respectively (Table S4). The loading state [C, S3, S2] is associated with transitions with low or marginal fluxes, including the seemingly direct switch from [C, S3, S2] to [S3, S2, S0], which decreases by about 1 order of magnitude compared to KcsA-WT. On the contrary, the probability of [S3, S2, S0] is 40 ± 2%, which is comparable with what was observed for the same state in KcsA-E71A. From this state, the transition with the highest net flux involves accommodating an ion in the cavity before S0 is vacated, leading to [C, S3, S2, S0], which eventually reaches the high probability state [S4, S2, S1]. This is consistent with the high ion occupancy of S4 and at the same time the lowest probability of finding a potassium ion in the cavity of TRAAK compared to the other investigated channels (Figure 2 and Table 1). Noteworthy, two other states hosting an ion in S4 are also ∼6% populated in TRAAK, [S4, S3, S1] and [S4, S2, S0], even though they are associated with very low net fluxes. State [S4, S2, S0] is of particular relevance, as it is not observed in the simplified networks of KcsA-WT and KcsA-E71A, and therefore it can be regarded as a TRAAK-specific state among the three channels. Overall, ion conduction in TRAAK is characterized by a dominant mechanism and a certain number of competing cycles. While this feature resembles the KcsAWT system, the population of the states and the magnitude of relative fluxes are strikingly dissimilar between the two channels (Tables S4 and S5), reflecting a distinct strategy of ion conduction.

The fact that TRAAK displays the highest S4 occupancy and the lowest probability of finding ions in the cavity calls for an in-depth analysis of the presence of lipid molecules inside the cavity, as this fact has been speculated to play a role in the gating mechanism of the channel.28,52 In Figure 5, how and to what extent lipid atoms can enter the cavity in a

representative simulation of the TRAAK channel performed at +200 mV is shown. A number of conduction events close to the average value collected from this set of simulations is displayed (replica #2, 8 conduction events; see also Table S3). Lipids can either reach the cavity from the fenestrations through their tails (first half of the run) or lean out of the inner mouth of the channel through their head groups (second half) as shown in Figure 5. Regardless of the presence of lipids, and even though lipid atoms occasionally almost reach the channel axis (distance always larger than 2 Å), the cavity remains hydrated enough to ensure a sustained diffusion of ions. Similar plots obtained at lower time resolution are shown in Figure S12 for all the replicas of the TRAAK channel. Notably, there is no apparent correlation between the presence of lipids in the cavity and the number of conduction events. For instance, only four conduction events are observed in replicas #1 and #12. However, in the former, lipids are never found within the cavity, while in the latter, lipids enter the cavity from both the fenestrations and the inner mouth. A similar scenario is observed for replicas #6 and #11, but, in this case, up to 10 conduction events were detected. Taken as a whole, this analysis suggests that the different occupancies observed for the TRAAK channel compared to KcsA wild type and mutant, as well as the lower conductance, cannot be solely ascribed to the presence of lipids inside the cavity, but should rather be regarded as distinctive features of the channel arising from its peculiar structure and dynamics.

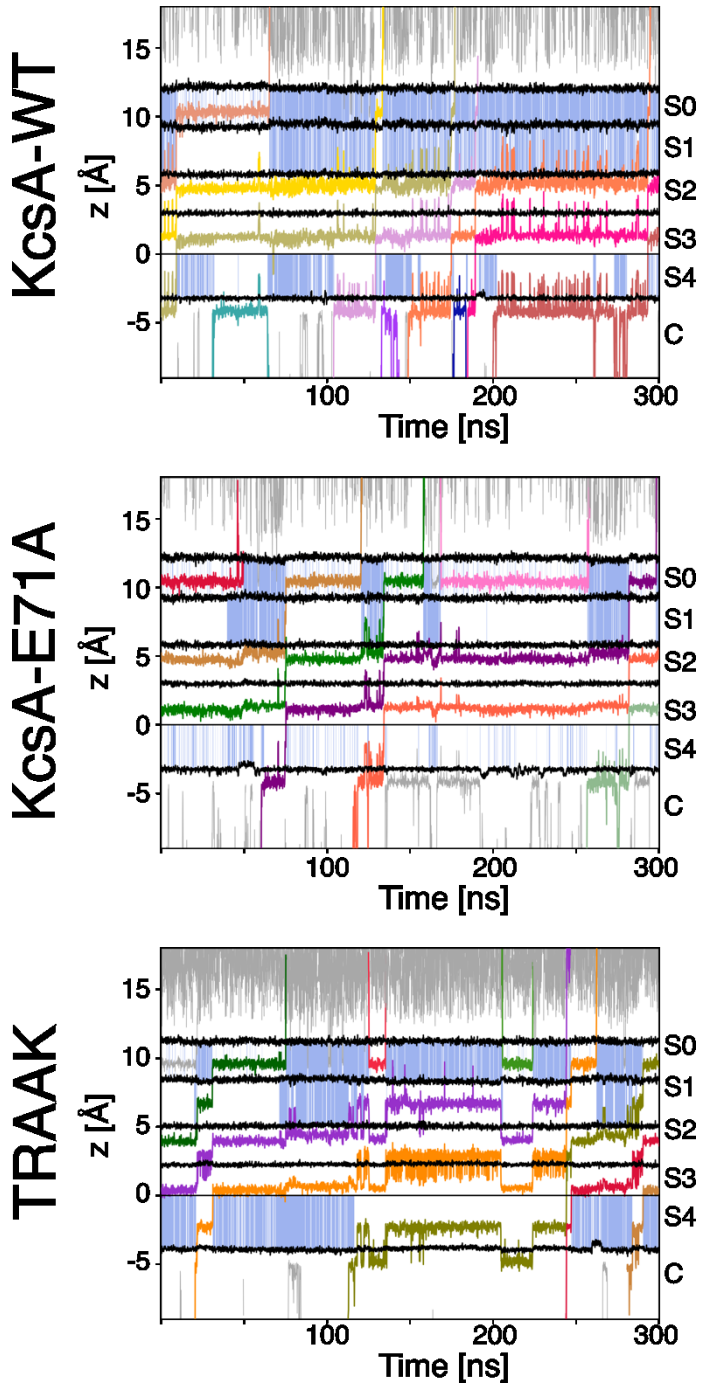

Figure 3. Examples of conduction events. Ion positions along the axis of the channel are shown for a 300 ns interval of one replica, using thin gray lines for the ions outside the selectivity filter and thick colored lines for the ions inside the selectivity filter. All the coordinates are referred to the center of mass of the carbonyl oxygen atoms of the threonine residues at the N-terminal of the SF (z = 0 Å). Thick black lines correspond to the center of mass of the oxygen atoms delimiting the binding sites. S0 to S4 labels indicate the positions of the ion binding site, and C indicates the channel cavity. Binding sites are shaded in light blue when occupied by at least one water molecule. In the case of KcsA-WT, the 300 ns interval was picked from the part of the trajectory after water had left the core of the SF.

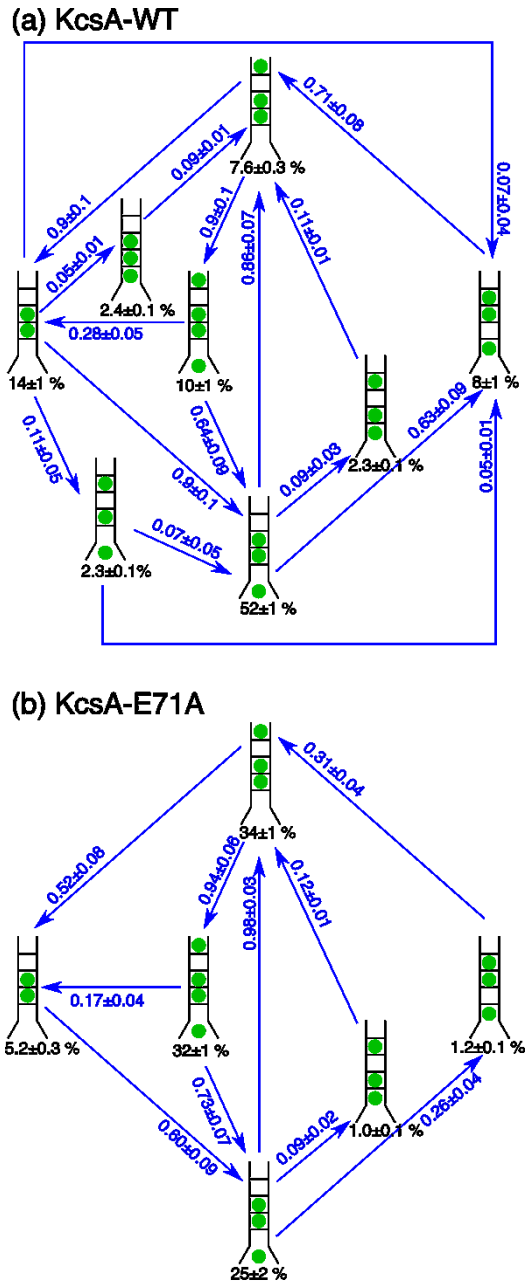
(a) KcsA-WT
7.6±0.3 %
0.71±0.08
0.09±0.01
0.9±0.1
0.07±0.04
0.05±0.01
0.9±0.1
0.11±0.01
0.86±0.07
2.4±0.1 %
0.28±0.05
14±1 %
10±1 %
8±1 %
0.11±0.05
0.64±0.09
0.63±0.09
0.09±0.03
2.3±0.1 %
0.05±0.01
0.9±0.1
2.3±0.1%
0.07±0.05
52±1 %
(b) KcsA-E71A
34±1 %
0.31±0.04
0.52±0.08
0.94±0.08
0.98±0.03
0.12±0.01
0.17±0.04
5.2±0.3 %
32±1 %
1.2±0.1 %
0.73±0.07
0.60±0.09
0.09±0.02
1.0±0.1 %
0.26±0.04
25±2 %
(c) TRAAK
0.99±0.01
0.06±0.03
40±2 %
0.37±0.09
0.85±0.07
0.07±0.05
0.18±0.02
0.12±0.02
5.7±1.2 %
0.68±0.05
9±2 %
5.9±0.8 %
27±4 %
0.15±0.02
0.05±0.02
0.26±0.06
0.05±0.03
0.07±0.03
5.9±0.7 %
0.30±0.07
0.08±0.03
1.0±0.2 %
3.7±0.7 %

Figure 4. Net fluxes between states of the selectivity filter. The occupancy state of the selectivity filter is schematically represented, with cavity at the bottom followed by S4-S0, and using green circles for potassium ions. The probability of the corresponding state is indicated below the schematic selectivity filter representation. Only the nodes with a probability greater or equal to 1% are shown. In order to facilitate comparisons, the same states are represented in the same relative positions for the three channel models. Blue arrows are used for the net fluxes, with labels providing the ratio between the net flux between that particular pair of nodes and the maximum net flux observed among any pair of nodes. The link between two states is shown only if the normalized net fluxes between the corresponding nodes is higher than 0.05.

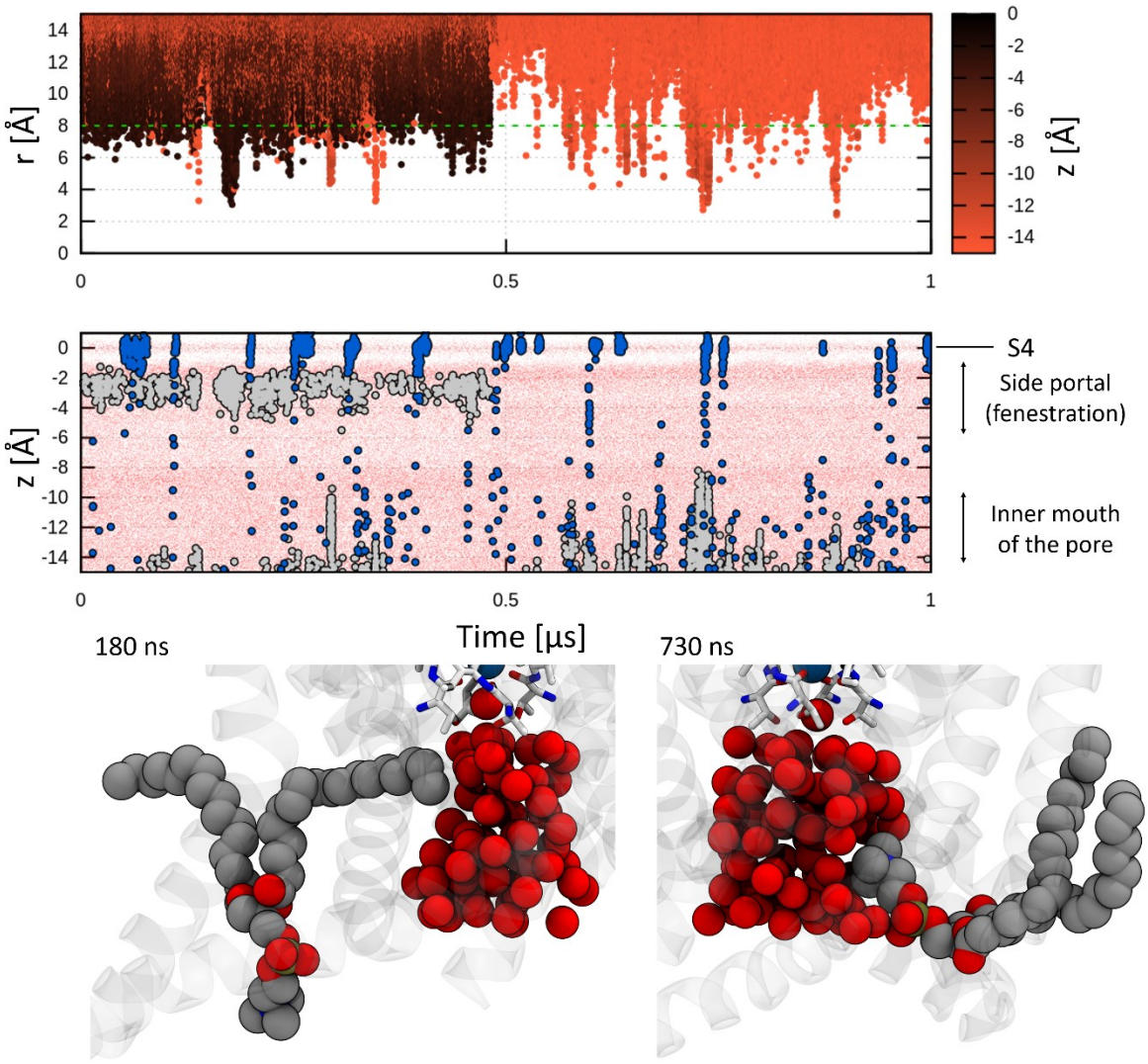

Figure 5. Lipids entering the cavity in the TRAAK channel. The presence of lipids inside the cavity of a representative simulation performed at +200 mV of the TRAAK channel (replica

#2) is shown by plotting the radial distance of every lipid atom with respect to the channel axis (top panel). The black-to-red color code refers to the position along the z-axis of the lipid atoms. The radius of 8 Å, which approximately corresponds to the radius of the cavity, is shown as a green dotted line. In the middle panel, the z-position of atoms belonging to water molecules, lipids, and potassium ions found within a radius of 8 Å from the channel axis are shown as red dots, gray circles, and blue circles, respectively. Two representative configurations extracted at 180 and 730 ns and displaying different modalities of lipid entering the cavity are also shown (bottom panel).

Conclusions

The different occupancy of the SF binding sites observed for KcsA-WT, KcsA-E71A, and TRAAK supports the hypothesis of a nonuniversal conduction strategy in K+-channels. Mechanisms of ion conduction have been extensively investigated in several other computational studies using the same channels considered in this study, as well as other members belonging to other families. It is therefore reasonable and imperative to compare our results with those previously reported in the literature. For the sake of clarity, we have limited the comparison of ion conduction to those studies in the absence of interposed water molecules, when the main SF configuration states are explicitly reported in the original source and when the starting configuration is clearly restored following a cycle of events.

KcsA has been largely studied because of its archetypical role in the field of potassium channels. Perhaps in this context, the most relevant work is the one reported by Köpfer et al. using membrane potentials ranging from +200 mV up to almost +600 mV.11 Similar to the dominant mechanism reported here, the authors identify the most populated SF configuration as the one with K+ ions at S2 and S3, while a more loosely bound ion was found at S0. Bernsteiner et al. have recently reported a thorough investigation of the inward rectifying Kir3.2 channel, including the study of ion conduction performed with an applied electric field corresponding to membrane potentials of +290 and +580 mV.53 In this case, the states of the SF involved in the mechanism of ion conduction are strikingly different to those identified as relevant states in this study. Most importantly, in the Kir3.2 channel, there is a marked presence of states with three consecutive potassium ions at [S4, S3, S2] and at [S2, S1, S0] that were observed with low probability in our simulations. Even though simulations of the Kir3.2 channel were performed with a high electric field, the applied voltage was of the same order of magnitude as that employed by Köpfer et al. for KcsA.11 Thus, while these studies cannot be directly

compared to our work, as we have lower membrane potentials, a comparison between them is pertinent. The fact that remarkably different mechanisms were reported for KcsA and Kir3.2 further supports our suggestion that the preferred mechanism of ion conduction is specific to each channel.

Once it is established that conduction mechanisms are channel specific, examination of how alternative strategies might correlate with the functional properties of the different channels can be investigated. For instance, the comparison between KcsA-WT and KcsA-E71A immediately suggests some correlation between the different conduction strategies of these two variants and their C-type inactivation characteristics. The link between the preferred loading state of the SF and C-type inactivation has been demonstrated by electrophysiological experiments and by structural information extracted from X-ray crystallography.21,22 MD simulations confirmed that, compared to the conductive state, the collapsed state of the SF associated with C-type inactivation has a lower affinity for ions,54,55 and that inactivation is promoted by an increase in the number of water molecules at the back of the SF.56 Recently, we showed that the hydration level of the SF influences its dynamic properties.49 In equilibrium MD simulations, the SF deviates more from the experimental conductive structure in the presence of water molecules in binding sites S2 and S3 compared to simulations in the absence of water at the same binding sites. In the present study, water molecules are found to reside longer at both S1 and S0 in KcsA-WT compared to KcsA-E71A. On average, the loading states of KcsA-WT are occupied by fewer ions and more water molecules than in KcsA-E71A. Considering the time scales currently accessible by MD simulations, it is not possible to observe C-type inactivation events directly. However, the high probability of finding water molecules inside the SF, and the concurrent lower probability of ions in the KcsA-WT system compared to KcsA-E71A, together with the observation that water molecules tend to destabilize the experimental conductive state of the SF, suggest that their diverging inactivation properties could be attributed to the different conduction strategies of KcsA-WT and KcsA-E71A.

Concerning the TRAAK channel, it is noticeable that many aspects of gating and inactivation of the K2P family of channels remain partly elusive.57–59 Unlike classical voltage-gated and inward rectifier channels, K2P channels lack the helix-bundle crossing gate. Nevertheless, a so-called “X-gate”, unrelated to the helix bundle, has been recently described for the TASK-1 channel with bound inhibitors.60 TRAAK channels are also devoid of any apparent voltage-sensing domain, even if some of them display voltage-dependent activation.61 According to

the emerging picture of their functionality, channels that belong to the TREK subfamily, including TREK-1, TREK-2, and TRAAK,57 can adopt two distinct conformational states determined by the relative position of the TM4 helix with respect to the TM2 helix of the opposite monomer.28,62,63 Specifically, TM4 can kink at about the center of the lipid membrane around the position of a glycine residue (Gly268 in TRAAK) that is highly conserved in many K+-channels. This leads to the so-called “up” and “down” conformational states. Notably, in the down state, a lateral side fenestration is open, bringing the lipid environment in contact with the water-filled cavity. In contrast, in the up state, the fenestration is sealed.28,63 Since channels that belong to the TREK subfamily are all mechanosensitive channels,59 and because the conformation of TM4 can be modulated by membrane stretch, the hypothesis is that the up and down states represent functional gating states of the channels.28,52 Notably, the role played by membrane tension in driving the down-to-up transition has been confirmed for the TREK-2 channel through MD simulations.31 For the TRAAK channel, a gating mechanism involving the entrance of lipid molecules through the lateral fenestration has been suggested28,52 and later investigated through multiscale simulations.64 According to this model, a lipid tail could reach the cavity when the channel adopts the down state, thus hampering the translocation of incoming ions by steric hindrance. Upon membrane stretch, the lipidic hindrance is supposed to be relieved, and the channels would revert to the up state with sealed fenestrations, displaying maximum conductance. MD and Brownian dynamics simulations showed that ion permeation can be significantly affected by lipid tails inside the cavity only in the case of substantial lipid involvement.64 The results presented here support such a model. Among the investigated channels, TRAAK displays the highest degree of occupancy of potassium ions at S4 and the lowest at the cavity. This suggests that an efficient translocation of ions from the cavity to the SF might be a requirement for effective conduction in this family of channels.

Despite the appeal of the simple lipid block model, the statistical relevance of lipid tails entering the cavity substantially so as to impair ion conduction remains to be assessed.64 In addition, this model of gating does not account for the fact that other channels belonging to the TREK subfamily (like TREK-2) can be activated in the absence of membrane stretch.65 According to a more recent and sophisticated model proposed for members of the TREK subfamily, membrane stretch can directly activate the SF, as it has been experimentally reported for TREK-1 and TREK- 2.65,66 In this case, the down-to-up transition triggered by

membrane stretch is somehow allosterically transmitted to the SF that would act as an activation gate, the C-type gate.59 This hypothetical mechanism has been investigated for the TREK-2 channel by massive MD simulations performed in both equilibrium67 and out-of-equilibrium conditions with an externally applied electric field corresponding to a potential of +400 mV.32 In the former work, a “pinched state” of the channel was suggested as the inactive conformation of the SF, and the decrease in the conductance magnitude observed in the down state of the channel was correlated with the occurrence of a water-stabilized carbonyl flip of the S3 site in the latter.32,67 More recently, a mechanism describing the coupling between the conformation of channels at the transmembrane level and the gate at the SF has been investigated for the MthK channel and extended to other SF-activated K+-channels like BK and K2P channels.68 Specifically, the threonine residues of each monomer composing the S4 site were found to be pulled away from each other, resulting in larger outward currents up to a level where the widening of the site was detrimental for ion conduction as a consequence of an increased probability of water molecules entering the SF.68 Even from this standpoint, the high occupancy of potassium ions at S4 suggested by our mechanistic model underscores the importance of this site in the functionality of the TRAAK channel. Interestingly, the S4 site in TRAAK has also been proposed to be involved in the voltage-sensing behavior of this channel.51 In this model, called a “flux-gating model”, the SF of TRAAK would adopt an ion depleted/inactive state at rest that could switch to an ion occupied/inactive state upon depolarization. After a fast ion translocation step, the SF enters in the conductive mode upon a relatively slow structural transition (flux activation) that reflects the voltage-independent kinetics of the channel activation. Even though the molecular details behind this mechanism are still unclear, the data support the idea that the S4 site might play a major role in the flux-gating model, as mutations at this site abolish voltage gating but not permeation per se.51

In this study, microsecond-long MD trajectories using several independent replicas of three channel models amounting to 100 μs were collected and analyzed, rendering MSMs to investigate ion conduction. The permeation mechanisms were recorded at ionic concentrations and membrane potentials resembling those adopted in experimental settings. Remarkably, the dominant conduction mechanisms turned out to be significantly different for each of the three channels. The effect of several well-established factors including the composition of the lipid bilayer, the ion concentration, the membrane potential, or other physical/chemical stimuli known to impact conduction was not considered in this study,

neither was the effect of the adopted force field. Inherent approximations of classical force fields, and in particular the absence of polarizable effects, are well-known shortcomings in the computer simulation of ion channels. Using more sophisticated models might well reshape some of the conclusions resulting from our study. Nevertheless, that the atomistic features of the conduction process are specific to each channel is likely a robust argument that justifies the functional diversity and heterogeneous features of the considered K+-channels. The method adopted in this study, based on MSMs, offers an efficient strategy to compare conduction mechanisms in potassium channels. In this way, it was possible to identify significant differences among KcsAWT, KcsA- E71A, and TRAAK, providing robust evidence that supports the hypothesis that conduction in potassium channels does not follow a unique mechanism, but that, instead, each channel is likely to adopt different conduction strategies that could be seen as a fingerprint. The application of similar computational strategies to other ion channels and/or experimental conditions might shed further light on the atomic details of conduction mechanisms and into how these microscopic features contribute to the diverse functional properties of ion channels. This work aims also at inspiring chemists and material scientists developing artificial ion channels with high transport selectivity for applications in photonic devices, bioimaging, sensors, therapeutic treatment, or desalinization among many other purposes in fields ranging from chemistry to material science and of course biochemistry. The rational design of synthetic channels can help us address complex and fascinating challenges, and understanding how natural ion channels work then becomes crucial.

Supporting Information. List of simulated trajectories (Tables S1-S3). Occupancy states of the SF and net fluxes (Tables S4-S5). Occupancy of the SF by ions and water molecules in simulations with membrane potential equal to 100 mV (Figure S1). Effects of mutation Glu71Ala on the SF of KcsA (Figures S2-S4). Relaxation times of the MSMs as a function of the lag-time (Figure S5). Complete and simplified graphs representing the transition matrixes of the MSMs (Figures S6-S11). Entrance of lipids in the cavity of TRAAK (Figure S12).

Acknowledgments. CD acknowledges PRACE for awarding access to computational resources in CSCS, the Swiss National Supercomputing Service, in the 17th and 20th Project Access Calls, and RES (https://www.bsc.es/) for access to its computational resources.

References

1. Sasaki, R., Sato, K., Tabata, K. V, Noji, H. & Kinbara, K. Synthetic Ion Channel Formed by Multiblock Amphiphile with Anisotropic Dual-Stimuli-Responsiveness. *J. Am. Chem. Soc.* **143**, 1348–1355 (2021).
2. Muraoka, T. *et al.* Mechano-Sensitive Synthetic Ion Channels. *J. Am. Chem. Soc.* **139**, 18016–18023 (2017).
3. Muraoka, T. *et al.* Reversible Ion Transportation Switch by a Ligand-Gated Synthetic Supramolecular Ion Channel. *J. Am. Chem. Soc.* **136**, 15584–15595 (2014).
4. August, D. P. *et al.* Transmembrane Ion Channels Formed by a Star of David [2]Catenane and a Molecular Pentafoil Knot. *J. Am. Chem. Soc.* **142**, 18859–18865 (2020).
5. Benke, B. P. *et al.* Iodide-Selective Synthetic Ion Channels Based on Shape-Persistent Organic Cages. *J. Am. Chem. Soc.* **139**, 7432–7435 (2017).
6. Aqvist, J. & Luzhkov, V. Ion permeation mechanism of the potassium channel. *Nature* **404**, 881–4 (2000).
7. Bernèche, S. & Roux, B. Energetics of ion conduction through the K+ channel. *Nature* **414**, 73–77 (2001).
8. Domene, C., Vemparala, S., Furini, S., Sharp, K. & Klein, M. L. The role of conformation in ion permeation in a K+ channel. *J. Am. Chem. Soc.* **130**, 3389–3398 (2008).
9. Domene, C. & Sansom, M. S. P. Potassium Channel, Ions, and Water: Simulation Studies Based on the High Resolution X-Ray Structure of KcsA. *Biophys. J.* **85**, 2787–2800 (2003).
10. Furini, S. & Domene, C. Atypical mechanism of conduction in potassium channels. *Proc. Natl. Acad. Sci.* **106**, 16074–16077 (2009).
11. Köpfer, D. A. *et al.* Ion permeation in K+ channels occurs by direct Coulomb knock-on. *Science (80-.).* **346**, 352–355 (2014).
12. Furini, S. & Domene, C. K+ and Na+ Conduction in Selective and Nonselective Ion Channels Via Molecular Dynamics Simulations. *Biophys. J.* **105**, 1737–1745 (2013).
13. Maffeo, C., Bhattacharya, S., Yoo, J., Wells, D. & Aksimentiev, A. Modeling and simulation of ion channels. *Chem. Rev.* **112**, 6250–6284 (2012).

14. Furini, S. & Domene, C. Computational studies of transport in ion channels using metadynamics. *Biochim. Biophys. Acta - Biomembr.* **1858**, 1733–1740 (2016).

15. Roux, B. Ion channels and ion selectivity Essays in Biochemistry Benoît. *Essays Biochem.* **61**, 201–209 (2017).

16. Morais-Cabral, J. H. H., Zhou, Y. & MacKinnon, R. Energetic optimization of ion conduction rate by the K+ selectivity filter. *Nature* **414**, 37–40 (2001).

17. Mironenko, A., Zachariae, U., de Groot, B. L. & Kopec, W. The Persistent Question of Potassium Channel Permeation Mechanisms. *J. Mol. Biol.* 167002 (2021) doi:10.1016/j.jmb.2021.167002.

18. Öster, C. *et al.* The conduction pathway of potassium channels is water free under physiological conditions. *Sci. Adv.* **5**, 3–9 (2019).

19. Iwamoto, M. & Oiki, S. Countingion and water molecules in a streaming file through the open-filter structure of the K channel. *J. Neurosci.* **31**, 12180–12188 (2011).

20. Kopec, W. *et al.* Direct knock-on of desolvated ions governs strict ion selectivity in K+ channels. *Nat. Chem.* **10**, 813–820 (2018).

21. López-Barneo, J., Hoshi, T., Heinemann, S. H. & Aldrich, R. W. Effects of external cations and mutations in the pore region on C-type inactivation of Shaker potassium channels. *Receptors Channels* **1**, 61–71 (1993).

22. Matulef, K., Annen, A. W., Nix, J. C. & Valiyaveetil, F. I. Individual Ion Binding Sites in the K+ Channel Play Distinct Roles in C-type Inactivation and in Recovery from Inactivation. *Structure* **24**, 750–761 (2016).

23. Doyle, D. A. *et al.* The structure of the potassium channel: molecular basis of K+ conduction and selectivity. *Science (80-.).* **280**, 69–77 (1998).

24. Chakrapani, S., Cordero-Morales, J. F. & Perozo, E. A quantitative description of KcsA gating I: Macroscopic currents. *J. Gen. Physiol.* **130**, 465–478 (2007).

25. Cordero-Morales, J. F. *et al.* Molecular determinants of gating at the potassium-channel selectivity filter. *Nat. Struct. Mol. Biol.* **13**, 311–318 (2006).

26. Brohawn, S. G., Campbell, E. B. & MacKinnon, R. Domain-swapped chain connectivity

and gated membrane access in a Fab-mediated crystal of the human TRAAK K+ channel. *Proc. Natl. Acad. Sci. U. S. A.* **110**, 2129–2134 (2013).

27. Cuello, L. G., Cortes, D. M. & Perozo, E. The gating cycle of a K+ channel at atomic resolution. *Elife* **6**, 1–17 (2017).

28. Brohawn, S. G., Campbell, E. B. & MacKinnon, R. Physical mechanism for gating and mechanosensitivity of the human TRAAK K+ channel. *Nature* **516**, 126–130 (2014).

29. Jo, S., Kim, T., Iyer, V. G. & Im, W. CHARMM-GUI: A web-based graphical user interface for CHARMM. *J. Comput. Chem.* **29**, 1859–1865 (2008).

30. Lomize, M. A., Pogozheva, I. D., Joo, H., Mosberg, H. I. & Lomize, A. L. OPM database and PPM web server : resources for positioning of proteins in membranes. **40**, 370–376 (2012).

31. Aryal, P. *et al.* Bilayer-Mediated Structural Transitions Control Mechanosensitivity of the TREK-2 K2P Channel. *Structure* **25**, 708-718.e2 (2017).

32. Brennecke, J. T. & de Groot, B. L. Mechanism of Mechanosensitive Gating of the TREK-2 Potassium Channel. *Biophys. J.* **114**, 1336–1343 (2018).

33. Oakes, V., Furini, S. & Domene, C. Effect of anionic lipids on ion permeation through the KcsA K+-channel. *Biochim. Biophys. Acta - Biomembr.* **1862**, 183406 (2020).

34. Jorgensen, W. L., Chandrasekhar, J., Madura, J. D., Impey, R. W. & Klein, M. L. Comparison of simple potential functions for simulating liquid water. *J. Chem. Phys.* **79**, 926–935 (1983).

35. Maier, J. A. *et al.* ff14SB: Improving the Accuracy of Protein Side Chain and Backbone Parameters from ff99SB. *J. Chem. Theory Comput.* **11**, 3696–3713 (2015).

36. Joung, I. S. & Cheatham, T. E. Determination of alkali and halide monovalent ion parameters for use in explicitly solvated biomolecular simulations. *J. Phys. Chem. B* **112**, 9020–9041 (2008).

37. Essmann, U. *et al.* A smooth particle mesh Ewald method. *J. Chem. Phys.* **103**, 8577–8593 (1995).

38. Tuckerman, M., Berne, B. J. & Martyna, G. J. Reversible multiple time scale molecular

dynamics. *J. Chem. Phys.* **97**, 1990–2001 (1992).

39. Feller, S. E., Zhang, Y., Pastor, R. W. & Brooks, B. R. Constant pressure molecular dynamics simulation: The Langevin piston method. *J. Chem. Phys.* **103**, 4613–4621 (1995).

40. Gumbart, J., Khalili-Araghi, F., Sotomayor, M. & Roux, B. Constant electric field simulations of the membrane potential illustrated with simple systems. *Biochim. Biophys. Acta - Biomembr.* **1818**, 294–302 (2012).

41. Khalili-Araghi, F., Ziervogel, B., Gumbart, J. C. & Roux, B. Molecular dynamics simulations of membrane proteins under asymmetric ionic concentrations. *J. Gen. Physiol.* **142**, 465–475 (2013).

42. Phillips, J. C. *et al.* Scalable molecular dynamics with NAMD. *J. Comput. Chem.* **26**, 1781–1802 (2005).

43. Michaud-Agrawal, N., Denning, E. J., Woolf, T. B. & Beckstein, O. MDAnalysis: a toolkit for the analysis of molecular dynamics simulations. *J. Comput. Chem.* **32**, 2319–2327 (2011).

44. Virtanen, P. *et al.* SciPy 1.0: fundamental algorithms for scientific computing in Python. *Nat. Methods* **17**, 261–272 (2020).

45. Humphrey, W., Dalke, A. & Schulten, K. VMD: visual molecular dynamics. *J. Mol. Graph.* **14**, 27-28,33-38 (1996).

46. Bowman, G. R., Pande, V. S. & Noé, F. *An introduction to Markov State Models and their application to long timescale molecular simulations*. (Springer Netherlands, 2014). doi:10.1007/978-94-007-7606-7.

47. Bastian, M., Heymann, S. & Jacomy, M. Gephi: An Open Source Software for Exploring and Manipulating Networks. (2009).

48. Ocello, R. *et al.* Conduction and Gating Properties of the TRAAK Channel from Molecular Dynamics Simulations with Different Force Fields. *J. Chem. Inf. Model.* **60**, 6532–6543 (2020).

49. Furini, S. & Domene, C. Critical Assessment of Common Force Fields for Molecular Dynamics Simulations of Potassium Channels. *J. Chem. Theory Comput.* **16**, 7148–7159

(2020).

50. Jensen, M. Ø., Jogini, V., Eastwood, M. P. & Shaw, D. E. Atomic-level simulation of current–voltage relationships in single-file ion channels. *J. Gen. Physiol.* **141**, 619–632 (2013).

51. Schewe, M. *et al.* A Non-canonical Voltage-Sensing Mechanism Controls Gating in K2P K+ Channels. *Cell* **164**, 937–949 (2016).

52. Brohawn, S. G., Su, Z. & MacKinnon, R. Mechanosensitivity is mediated directly by the lipid membrane in TRAAK and TREK1 K+ channels. *Proc. Natl. Acad. Sci. U. S. A.* **111**, 3614–3619 (2014).

53. Bernsteiner, H., Zangerl-Plessl, E. M., Chen, X. & Stary-Weinzinger, A. Conduction through a narrow inward-rectifier K+ channel pore. *J. Gen. Physiol.* **151**, 1231–1246 (2019).

54. Domene, C. & Furini, S. Dynamics, Energetics, and Selectivity of the Low-K+ KcsA Channel Structure. *J. Mol. Biol.* **389**, 637–645 (2009).

55. Furini, S., Beckstein, O. & Domene, C. Permeation of water through the KcsA K + channel. *Proteins Struct. Funct. Bioinforma.* **74**, 437–448 (2009).

56. Li, J., Ostmeyer, J., Cuello, L. G., Perozo, E. & Roux, B. Rapid constriction of the selectivity filter underlies C-type inactivation in the KcsA potassium channel. *J. Gen. Physiol.* **215**, 1408–1420 (2018).

57. Feliciangeli, S., Chatelain, F. C., Bichet, D. & Lesage, F. The family of K2P channels: salient structural and functional properties. *J. Physiol.* **593**, 2587–2603 (2015).

58. Niemeyer, M. I., Cid, L. P., González, W. & Sepúlveda, F. V. Gating, Regulation, and Structure in K2P K+ Channels: In Varietate Concordia? *Mol. Pharmacol.* **90**, 309–317 (2016).

59. Douguet, D. & Honoré, E. Mammalian Mechanoelectrical Transduction: Structure and Function of Force-Gated Ion Channels. *Cell* **179**, 340–354 (2019).

60. Rödström, K. E. J. *et al.* A lower X-gate in TASK channels traps inhibitors within the vestibule. *Nature* **582**, 443–447 (2020).

61. Enyedi, P. & Czirják, G. Molecular background of leak K+ currents: two-pore domain potassium channels. *Physiol. Rev.* **90**, 559–605 (2010).

62. Brohawn, S. G., Campbell, E. B. & MacKinnon, R. Domain-swapped chain connectivity and gated membrane access in a Fab-mediated crystal of the human TRAAK K+ channel. *Proc. Natl. Acad. Sci. U. S. A.* **110**, 2129–2134 (2013).

63. Dong, Y. Y. *et al.* K2P channel gating mechanisms revealed by structures of TREK-2 and a complex with Prozac. *Science (80-.).* **347**, 1256–1259 (2015).

64. Masetti, M. *et al.* Multiscale Simulations of a Two-Pore Potassium Channel. *J. Chem. Theory Comput.* **12**, 5681–5687 (2016).

65. McClenaghan, C. *et al.* Polymodal activation of the TREK-2 K2P channel produces structurally distinct open states. *J. Gen. Physiol.* **147**, 497–505 (2016).

66. Lolicato, M. *et al.* K2P2.1 (TREK-1)-activator complexes reveal a cryptic selectivity filter binding site. *Nature* **547**, 364–368 (2017).

67. Harrigan, M. P., McKiernan, K. A., Shanmugasundaram, V., Denny, R. A. & Pande, V. S. Markov modeling reveals novel intracellular modulation of the human TREK-2 selectivity filter. *Sci. Rep.* **7**, 1–8 (2017).

68. Kopec, W., Rothberg, B. S. & de Groot, B. L. Molecular mechanism of a potassium channel gating through activation gate-selectivity filter coupling. *Nat. Commun.* **10**, 5366 (2019).

TABLE OF CONTENT GRAPHICS